Coherent and Broadband Enhanced Optical Absorption in Graphene

Giuseppe Pirruccio,[*,†] Luis Martin Moreno,[‡] Gabriel Lozano,[†] and Jaime Gomez Rivas[†,¶]

FOM Institute for Atomic and Molecular Physics AMOLF, c/o Philips Research Laboratories, High Tech Campus 4, 5656 AE, Eindhoven, The Netherlands, Instituto de Ciencia de Materiales de Aragon and Departamento de Fisica de la Materia Condensada, CSIC-Universidad de Zaragoza, E-50009 Zaragoza, Spain, and COBRA Research Institute, Eindhoven University of Technology, P.O. Box 513, 5600 MB Eindhoven, The Netherlands.

E-mail: pirruccio@amolf.nl

Keywords: Graphene; enhanced absorption; photodetection; coherent absorption; control;

Abstract

We experimentally demonstrate a broadband enhancement of the light absorption in graphene over the whole visible spectrum. This enhanced absorption is obtained in a multilayer structure by using an Attenuated Total Reflectance (ATR) configuration and it is explained in terms of coherent absorption arising from interference and dissipation. The interference mechanism leading to the phenomenon of coherent absorption allows for its precise control by varying the refractive index and/or thickness of the medium surrounding the graphene.

---

[*]To whom correspondence should be addressed
[†]FOM institute AMOLF
[‡]CSIC - University of Zaragoza
[¶]TUe

Graphene, a truly 2-dimensional gapless semiconductor, has been recognized as a revolutionary material for opto-electronic applications. Several applications of graphene in various devices have been proposed, such as transparent electrodes,[1,2] ultrafast lasers,[3] polarizers,[4] and photodetectors.[5] At optical frequencies graphene behaves as an absorbing dielectric due to the onset of interband transitions, which leads to a negative imaginary component of its optical conductivity and a real component that approaches the universal conductivity value.[6] Photon absorption through interband transitions leads to the formation of electron-hole pairs, which are essential to build up an electric signal associated to the photodetection process. The low absolute value of the absorption of graphene (2.3% of the incident light is absorbed in a graphene layer[7]) constitutes the main limitation for the photocurrent efficiencies of graphene-based photodetectors.[5,8] Therefore one of the challenges concerning this ultra-thin material is to enhance its optical absorption.[9,17] In general, enhancing and controlling light absorption in optical devices is receiving significant attention due to the increasing interest in its fundamental and practical aspects.[10–16] Typical parameters to be optimized are the spectral and angular window of illumination over which the enhanced absorption takes place and its dependence on the polarization of the incident light. The optical absorption of graphene integrated in silicon waveguides has been recently demonstrated by Liu *et al.*[18] and by Li *et al.*[19] A way to increase the photocurrent in graphene-based detectors has been demonstrated by M. Furchi *et al.* by integrating the graphene in a microcavity defined by a pair of Bragg mirrors.[20] Engel *et al.*[21] used the cavity defined by metallic mirrors to enhance the photocurrent of a graphene-based transistor. These approaches lead to a large enhancement of the optical absorption in a limited range of wavelengths (~ 50 nm) and angles of incidence. A detailed theoretical description of a graphene integrated microcavity has been accomplished by Ferreira and coauthors.[22] A plasmonic-assisted enhancement of the electric field near the contacts of a graphene-based photodetector has been exploited by Echtermeyer *et al* to enhance the photovoltage.[23] Also the possibility to achieve complete absorption in graphene at infrared frequencies making use of plasmonic resonances has been theoretically investigated in nanopatterned graphene by Thongrattanasiri *et al.*[24]

In this manuscript we demonstrate a simple, yet robust, configuration to achieve a remarkably large, broadband and polarization independent absorption of visible light in graphene. This enhanced absorption is achieved by interference and dissipation in a four layers structure. One of these layers is a graphene monolayer or multilayer (depending on the sample). The graphene is sandwiched between two non-absorbing dielectrics with slightly different refractive indexes. Light impinges onto this structure through a high refractive index prism at a large angle of incidence. Destructive wave interference builds up in reflection, while the optical transmission vanishes due to total internal reflection. The coherent suppression of reflection and transmission translates into an enhancement of the graphene's absorption. In contrast to previous works, this simple structure enables a broadband enhancement of the absorption in a narrow window of angles of incidence. We experimentally show an absorptance higher than 10% for a monolayer of graphene over a range of wavelengths spanning from 525 till 800 nm. This absorption increases to 60% and 70% for 5 and 10 layers of graphene, respectively. We also show how the absorption of the 10 graphene layers can be optimized to reach values as large as 91%. Moreover, the absorption can be precisely controlled by changing the difference in refractive indices of the dielectrics embedding the graphene.

Sample characterization

Three samples were prepared in order to investigate the enhanced absorption in graphene: The first one is formed by 10 layers of graphene, the second by 5 layers of graphene and the third by a monolayer. The multilayers were made by turbostratic deposition (see Methods). Raman measurements (see discussion below) show that these multilayers have a net graphene behavior and do not form graphite. Figure 1(a) displays the optical characterization of the three samples through absorptance measurements in an integrating sphere at normal incidence. The absorptance is defined as 1-R_T-T_T, with R_T and T_T the total reflectance and total transmittance, respectively. The open circles, squares and triangles correspond to the measurements of 10, 5 and 1 graphene layers, respectively. The small bump at $\lambda = 700$ nm is due to residual absorption from impurity

iron particles involved in the deposition process of the graphene. The solid curves in Fig. 1(a) are fits to the measurements using the transfer matrix method. For these fits, we model the samples as a 3 layers system, consisting of a substrate, the graphene layer and air. The absorption band of the iron particles is not included in the model and we consider the silica substrate to be non-dispersive with a permittivity $\varepsilon_{sub} = 2.08$. The graphene (multi-)layer can be described as a uniaxial material, characterized by an ordinary in-plane permittivity and by an extraordinary out-of-plane permittivity.[25] Since the absorptance measurements in Fig. 1 (a) are performed at near normal incidence, the graphene layers are described only through the ordinary permittivity. The birefringence will be later taken into account when measurements at an inclined angle of incidence are discussed. The ordinary refractive index is related to the optical conductivity, σ, by $\varepsilon_o = 4\pi i \sigma / \omega h$, where ω is the frequency of the incident wave and h is the thickness of the graphene layer. The permittivities of the graphene layers at 540 nm obtained from the fits to the transmission and reflection measurements are $\varepsilon_o = (5.9 \pm 0.8) + i(10.2 \pm 0.6)$, $(7.8 \pm 0.8) + i(8.5 \pm 0.4)$ and $(7.1 \pm 3.2) + i(7.9 \pm 1.4)$ for 10, 5 and 1 graphene layers. These values are in reasonable agreement with $\varepsilon_o = 5.6 + i7.0$ reported by Kravetz et al.[25] and the absorptance is consistent with the well known value of 2.3% per graphene layer predicted by Kuzmenko et al.[7] The discrepancy in the permittivity between measurements and reported values, which in the worst case is around 30%, can be attributed to differences in the fabrication process and the aforementioned impurities present in our samples.

To confirm the behavior of the graphene multilayers as a stack of monolayers (instead of thin graphite sheet), we have performed Raman spectroscopy. It is known that the frequency of the G-Raman line, the intensity of the D-Raman line, the relative intensity of the G- and 2D-Raman lines and the line shape of the 2D-line give a valuable indication of the quality of graphene.[26] The black, dark grey and light grey curves in Fig. 1(b) are Raman spectra obtained under a 514 nm illumination of 10, 5 layers and the monolayer of graphene, respectively, where the first two have been vertically displaced for clarity. We see the following features as a function of the number of graphene layers: i) the intensity of the 2D-line is always larger than the intensity of the G-line, ii) the intensity of the D-line remains low, and (iii) the 2D-line maintains a lorentzian-like

shape. These observations provide an excellent indication that all the samples have a net graphene-like behavior and do not form graphite. As expected the intensity of the Raman signal increases with the number of graphene layers.[28] The fact that a graphene behavior is found even for the 10 layer sample can be explained by considering the random relative alignment of the stacked layers resulting from the deposition. The frequency shift of the G-line is known to provide information about the number of graphene layers stacked together.[27–29] In Fig. 1(c) we desplay 4 spectra taken from different locations in the sample with 10 layers of graphene for which imperfections due to the layer by layer deposition could be more important. The identical Raman frequency of the G-line confirms that the sample is homogeneous.

Results and discussion

In order to demonstrate the coherent and enhanced absorption in graphene multilayers, we have built the structure schematically represented in Fig. 2 (a). A silica layer with a defined thickness on the order of the wavelength of the incident light and permittivity $\varepsilon_{silica} = 2.12$ is sputtered on top of the graphene. The permittivity of the silica layer has been chosen to be very close but slightly larger than the one of the quartz substrate ($\varepsilon_{subs} = 2.08$). A prism made of F2 glass with a permittivity $\varepsilon_p \sim 2.59$ and slightly dispersive in the visible, is used to couple the incident light into the multilayer structure. This is the standard Attenuated Total Reflectance (ATR) configuration in which the refractive index of the prism has to be higher than the refractive index of the substrate in order to allow for total internal reflection of the incident light. A similar configuration has been theoretically modeled by Bludov and coauthors to enhance the absorption of THz (far-infrared) by graphene .[30,31] In that work the authors exploit an evanescent coupling through a prism to excite graphene surface plasmon polaritons. Note that our work focuses on the visible part of the spectrum where graphene exhibits a dielectric behaviour and do not support surface plasmons. The total internal reflection prevents the light to be scattered in the transmission far-field for angles of incidence θ larger than the critical angle. The critical angle angle for total internal reflection at the

prism-silica interface is

$\theta_{c,1} = \arcsin(\sqrt{\varepsilon_{silica}}/\sqrt{\varepsilon_p})$, while the critical angle for total internal reflection at the silica-substrate interface is $\theta_{c,2} = \arcsin(\sqrt{\varepsilon_{sub}}/\sqrt{\varepsilon_{silica}})$. These interfaces are labeled with 1 and 2, respectively, in Fig. 2(a). The angle of incidence θ^* on the prism-silica interface corresponding to $\theta_{c,2}$ can be evaluated applying the Snell law, *i.e.*, $\sqrt{\varepsilon_p} \cdot \sin(\theta^*) = \sqrt{\varepsilon_{silica}} \cdot \sin(\theta_{c,2})$. If $\theta < \theta^*$ the incident wave propagates through the multilayer structure and a fraction of the amplitude is transmitted. When $\theta^* < \theta < \theta_{c,1}$ the incident wave is transmitted through the prism-silica layer interface and undergoes total internal reflection at the silica-substrate interface. If $\theta > \theta_{c,1}$ the wave undergoes total internal reflection at the prism-silica interface. Therefore, the last two conditions result in a transmittance equal to 0.

Specular reflectance (R) measurements have been performed for the three samples. The measurements are normalized to the specular reflection at an angle of incidence of $\theta = 65.3° > \theta_{c,1}$, at which a reflectance of 1 is expected due to total internal reflection at the prism-silica interface. For $\theta > \theta^*$ the absorptance is defined as A=1-R. Figure 2 (b) displays the experimental absorptance of the 5 layers of graphene as a function of the wavelength and the angle of incidence for p-polarized incident light at $\theta > \theta^*$. The measurements of the monolayer of graphene and the 10 layers of graphene are shown in Fig. S1 of the supplementary information. The red and pink dashed lines in Fig. 2 (b) represent the dispersion of θ^* and $\theta_{c,1}$, respectively. Following the dispersion of θ^* we see a band in which the absorptance reaches values as large as 0.75. This band of enhanced absorptance covers the whole visible spectrum from 460 nm to 800 nm. The large absorption enhancement is independent of polarization and similar results are obtained under s-polarized illumination (see Fig. S2 in supplementary). To better visualize the absorption enhancement, the averaged absorptance over a narrow range of angles of incidence ($\Delta\theta \simeq 0.05$ °) is plotted in Fig. 2 (c) as a function of the wavelength. The blue circles correspond to the angular window identified by the dashed vertical lines in Fig. 2 (b). The other absorptance spectra are obtained in a similar way for different angular ranges. We see over the whole visible spectrum an experimental absorptance at certain angles of incidence larger than 60%, *i.e.*, pronouncedly larger than the

11.5% expected for 5 layers of graphene and measured in Fig. 1 (a). The steep dispersion of the absorption band gives rise to a broadband enhanced absorption mainly in the red and near infrared part of the spectrum around 64.5°. The bandwidth of enhanced absorption is further improved for the 10 graphene layers sample where an absorptance larger than 70% is measured from 525 nm until 800 nm at θ=64.7° (see Fig. S1 (a) and S3 in the supplementary information). It is worth noting that a thin layer of an absorbing material in a symmetric environment cannot absorb more than 50% of the incident light.[24] Therefore, the presence of the asymmetry in the permittivity of the surrounding media is crucial to boost the absorption of the graphene.

Figure 3 (a) displays the measured absorptance as a function of the incident angle for a p-polarized illumination wavelength of 540 nm and for the 10 graphene layers (open circles), the 5 graphene layers (open squares), and the monolayer (open triangles) of graphene, respectively. In Fig. 3 (b) is plotted the calculated absorptance evaluated by means of the transfer matrix method for the same layers, polarization and illumination wavelength of the measurements, *i.e.*, for 10 (solid black curve), 5 (dashed dark-grey curve), and 1 layer (dot-dashed light-grey curve) and p-polarized light of λ =540 nm. The calculations model the layers through their thicknesses and permittivities assuming them as perfectly flat. The thicknesses and the permittivity of the silica layer have been determined by ellipsometry measurements. These thicknesses of the silica layers are 590 nm, 1200 nm and 1300 nm for the 10 layers, 5 layers and monolayer of graphene samples, respectively. We model the graphene as a uniaxial material with a complex permittivity $\varepsilon_g(\lambda, \theta) = \varepsilon_o(\lambda) + \frac{\varepsilon_o(\lambda) - \varepsilon_e(\lambda)}{\varepsilon_e(\lambda)} sin^2\theta$, where $\varepsilon_o(\lambda)$ is the complex ordinary permittivity, and $\varepsilon_e(\lambda)$ is the complex extraordinary permittivity, fixed to the value of $3.9 + i0.7$ as determined in Ref.[25] The complex ordinary permittivity of graphene is taken from the fits shown in Fig. 1(a). Therefore, no fitting parameter is used in the calculations shown in Fig. 3 (b). The discrepancy between the measurements and the calculations in the strength of the absorption can be attributed to the presence of the aforementioned impurity particles on the surface of the graphene and to a possible small modification of the optical constants of the graphene layers caused by the deposition of the silica layer. Nevertheless, these calculations reproduce perfectly the shape and the angular position

of the absorption resonances of the three samples.

The enhanced absorptance observed in the measurements, and qualitatively reproduced by the transfer matrix calculations, is associated with the excitation of a resonance in the multilayer structure. To gain physical insight, the experiment can be described as a scattering problem, *i.e.*, as an incident beam traveling in a medium with permittivity ε_p and scattered (transmitted and reflected) by the multilayer. The scattering matrix, S, relates the asymptotic incoming and outgoing amplitudes of the reflected and transmitted waves. The scattering matrix can be obtained by solving Maxwell equations in each medium and applying the continuity of the tangential components of the fields at each interface. This results in

$$S = \begin{pmatrix} S_{11} & S_{12} \\ S_{21} & S_{22} \end{pmatrix} = \begin{pmatrix} t_{1234}^p & r_{4321}^p \\ r_{1234}^p & t_{4321}^p \end{pmatrix}, \tag{1}$$

where $r_{1234}^p, t_{1234}^p, r_{4321}^p, t_{4321}^p$ are the reflection and transmission Fresnel coefficients for p-polarization for the 4-layer system and the subindices 1, 2, 3 and 4, label the prism, the silica layer, the graphene (multi-) layer and the substrate, respectively. The Fresnel coefficients are given by [32]

$$r_{ijkl}^p = \frac{r_{ij}^p + r_{jkl}^p e^{-2\alpha_j d_j}}{1 + r_{ij}^p r_{jkl}^p e^{-2\alpha_j d_j}}; \qquad t_{ijkl}^p = \frac{t_{ij}^p t_{jkl}^p e^{-\alpha_j d_j}}{1 + r_{ij}^p r_{jkl}^p e^{-2\alpha_j d_j}}. \tag{2}$$

Where d_j is the thickness of the $j-th$ layer, r_{ij}^p and t_{ij}^p are the Fresnel reflection and transmission coefficients for the single interfaces, which are given by

$$r_{ij}^p = \frac{\varepsilon_j \alpha_i - \varepsilon_i \alpha_j}{\varepsilon_j \alpha_i + \varepsilon_i \alpha_j}, \qquad t_{ij}^p = \frac{2\sqrt{\varepsilon_i \varepsilon_j} \alpha_i}{\varepsilon_j \alpha_i + \varepsilon_i \alpha_j}, \tag{3}$$

with ε_i the permittivity of the medium i, and α_i is the component of the wavevector perpendicular to the interfaces, *i.e.*,

$$\alpha_i = \frac{2\pi}{\lambda} \sqrt{\varepsilon_1 sin^2 \theta - \varepsilon_i}. \tag{4}$$

r_{jkl}^p and t_{jkl}^p in Eq. (2) are the Fresnel coefficients of the system composed of layers j, k, l, given by

$$r_{jkl}^{p} = \frac{r_{jk}^{p} + r_{kl}^{p}e^{-2\alpha_k d_k}}{1 + r_{jk}^{p}r_{kl}^{p}e^{-2\alpha_k d_k}}; \qquad t_{ijkl}^{p} = \frac{t_{jk}^{p}t_{kl}^{p}e^{-\alpha_k d_k}}{1 + r_{jk}^{p}r_{kl}^{p}e^{-2\alpha_k d_k}}. \tag{5}$$

With these definitions, S_{21} relates the reflected amplitude, H_r, with the incident amplitude, H_i, of the magnetic field. Therefore, $|S_{21}|^2$ is the specular reflectance (R) that we measure. In particular for $\theta > \theta^*$ for which the transmittance vanishes, a minimum in $|S_{21}|^2$ corresponds to a maximum in the graphene absorptance. The zeros of S_{21} correspond to the condition of perfect antireflection resulting from Fabry-Pérot modes at which the phases and the amplitudes of the scattered waves at each interface are such that R approaches 0. In order to achieve antireflection, the reflected wave at the prism-silica interface needs to have a phase difference of 180° with the scattered wave from the other interfaces. This condition is necessary to obtain destructive interference in reflection. Assuming an amplitude of 1 for the incident wave, the amplitude and phase of the aforementioned scattered wave are given by $r_{scatt} = r_{1234}^{p} - r_{12}^{p}$. This out-of-phase condition can be controlled by a proper choice of the thickness of the silica layer over which the scattered wave accumulates a phase. Therefore, the optimum thickness of the silica layer can be evaluated by finding the minimum of $|S_{21}|^2$ as a function of the thickness of the silica layer and of the angle of incidence. For the sample with 10 layers of graphene and using the values for the permittivity of graphene obtained from the fits of Fig. 1, we find $d_{silica,opt} = 1.7\mu$m, for λ=540 nm and $\theta = 65.6°$. With this thickness we find $r_{scatt} = 0.9e^{-i173°}$, which is almost perfectly out-of-phase with $r_{12}^{p} = 0.7e^{i0°}$. It is important to note that a perfect destructive interference pattern, *i.e.*, perfect antireflection, is only possible if the absolute value of the amplitudes of r_{scatt} and r_{12}^{p} are equal. The role of the graphene (multi-) layer is to account for this amplitude condition by removing energy from the wave scattered by the multilayer. In the optimized case the absorptance in the 10 layers of graphene is 91%. However, it was not possible in the experiments to reach the optimum thickness of the silica layer with the method used for the growth (see Methods). Regarding the samples with 5 layers and the monolayer of graphene, a similar analysis leads to a maximum absorptance in the graphene of 76% and 15%, respectively. This means that the 5 graphene layers and the monolayer do not absorb enough energy and the matching condition for the amplitudes is not satisfied in order

9

to achieve full absorption. At this point it is worth mentioning that another way to exploit Fabry-Pérot resonances has been demonstrated by Blake *et al.* for making graphene more easily visible under a microscope.[33]

The analysis of the optical absorption in terms of the scattering matrix has been recently exploited to describe the concept of Coherent Perfect Absorption (CPA).[34–36] According to this description a proper combination of interference and dissipation in a weakly absorbing slab, giving rise to eigenvalues of S equal to zero, lead to complete absorption of the incident light. This perfect absorption has been interpreted as the time reversal of a lasing mode. The CPA process is associated in Ref.[35] to the superposition of two Fabry-Pérot of counter propagating beams. Following this description, the ATR configuration described here article could potentially represent a route towards the realization of one input channel CPA.[37]

Another way to increase the absorptance in graphene could be to exploit the coupling of the incident light to guided modes supported by the multilayer structure. The scattering matrix formalism can be used to obtain the dispersion relation of such modes by evaluating the poles of the S_{21}. The only guided modes supported by a graphene layer in the visible are the TE surface plasmon polariton,[38,39] while guided modes in the silica layer are not allowed because $\varepsilon_p > \varepsilon_{silica}$. Consequently, this approach can not be used in our system to enhance the absorption of p-polarized light.

Figure 3 (c) displays the spatial distribution of the intensity of the total electric field $|E|^2$, normalized by the incident intensity, in the multilayer system formed by the 5 layers of graphene for an incident wavelength and angle of $\lambda = 540$ nm and $\theta = 64.3°$, *i.e.*, for the wavelength and angle of incidence of maximum absorptance shown in Figs. 3(a) and (b). From top to bottom, Fig. 3(c) shows the prism (semi-infinite), the silica layer (1200 nm), the graphene multilayer (solid line) and the substrate (semi-infinite). The largest intensities are found in the silica and in the graphene layers. In Fig. 3(c) we also plot a cut of $|E|^2$ (green curve), showing the different behavior of the field in reflection and in transmission. Since the angle of incidence is such that $\theta^* < \theta < \theta_{c,1}$ (see Fig. 2 (b)), the electromagnetic field is evanescent in the substrate but propagating in the

silica layer and in the prism. The large intensity enhancement in the absorbing layer of graphene and the aforementioned destructive interference in reflection, explain why a resonance in a simple multilayer can boost the absorption of graphene.

The interference nature of the resonance giving rise to the enhanced absorption offers the opportunity to modulate this absorption. By tuning the permittivity of the media embedding the graphene layer is possible to modify the interference conditions, allowing part of the light to be reflected, and reducing the absorption. This tunability of the absorption is illustrated in Fig. 4. Figure 4 (a) shows the calculated absorptance for the 5 graphene layers sample. The transmittance and specular reflectance are evaluated with the transfer matrix method using the permittivities as in Fig 3. Figure 4(b) shows the calculated absorptance for the same set of permittivities as in Fig. 4 (a) but with $\varepsilon_{silica} = 2.15$ (instead of 2.12). The resonance shifts to larger angles and the absorptance decreases. Figures 4 (c) and (d) further illustrate how tuning the permittivities of the media surrounding the graphene allows for the control of the fraction of absorbed light at specific angles. These figures show the averaged absorptance obtained from Figs. 4 (a) and (b), respectively, over the same angular ranges as in Fig. 2 (c). The shift in the resonance as the permittivity of the silica layer is varied leads to a strong reduction of the absorptance at fixed wavelengths (see Fig. 4 (d)).

Conclusions

In conclusion, we have experimentally demonstrated a broadband enhancement of light absorption by graphene at optical frequencies by using an attenuated total reflection configuration in a simple multilayer structure. This broadband enhanced absorption is explained in terms of coherent absorption, which arises from the interference and dissipation in a multilayer structure. The engineered optical interference gives rise to a large electric field intensity in the proximity to the graphene layer, which is thereby dissipated.

METHODS

Samples fabrication

The graphene was grown by the company GrapheneSupermarket,[40] by chemical vapor deposition on copper foil and deposited, through PMMA transfer, onto a silica substrate. The PMMA was removed with acetone.[41] This process was repeated as many times as layers were deposited. The stacking of the multi-layer samples is turbostratic, which means that the layers are randomly aligned, thus preserving the graphene properties. The silica layer grown on top of the graphene is deposited through magnetron sputtering. The layer is grown in steps, *i.e.*, alternating two minutes of deposition with two minutes of cooling, in order to keep the temperature of the sample around 70°C. The deposition rate is 3.6 nm/min. The prism used for the ATR experiment is a EDP-50.0 from Melles Griot BV made of N-F2, with a refractive of 1.62 at a wavelength of 633 nm. The prism is in optical contact with the silica layer by means of an optical grade liquid (series A from Cargille labs), with a refractive index that matches the refractive index of the prism.

Raman Characterization

The microscope used for the Raman analysis is a Ranishaw InVia. An Ar+ laser is used as a source operating at the wavelength of 514 nm. The estimated power on the sample is 20 mW. The objective used has a 100x magnification and NA=0.9. The grating of the spectrometer has 2400 lines/mm.

Optical Measurements

The absorptance shown in Fig. 1 (a) are obtained from the measurements of the total reflectance and total transmittance. These measurements were done using a Lambda 950 spectrophotometer (PerkinElmer) consisting of a tungsten-halogen and a deuterium lamp, an integrating sphere, and a photomultiplier tube. For the reflectance measurements, the samples were mounted at the backside of the integrating sphere, while for the transmittance measurements the samples were mounted at the frontside of the sphere. The measurements are normalized using a white-standard.

The angle-resolved specular reflectance measurements shown in Figs. 3 and 4 are performed in

a computer controlled rotation stage, which allows for the independent movement of the detector (a fiber-coupled Ocean Optics 2000+ spectrometer) and the sample. The step of rotation of the sample is 0.05°.

Acknowledgement

Supporting Information Available   Measured specular reflectance as a function of wavelength and angle of incidence for p-polarized light for the three samples; Experimental absorptance of p-polarized light measured at 64.7° of 10 layers of graphene; Measured specular reflectance for s-polarized light of the multilayer system with 5 layers of graphene. These information is available free of charge *via* the Internet at http://pubs.acs.org.

References

1. Gilje, S.; Han, S.; Wang, M.; Wang, K. L.; Kaner R. B. A Chemical Route to Graphene for Device Applications, *Nano Lett.*, **2007**, 7, 3394-3398.

2. Bae,S.; Kim, H.; Lee, Y.; Xu, X.; Park, Y.; Zheng, Y.; Balakrishnan, J.; Lei, T.; Kim, H. R.; Song, Y. I.; *et al.* Roll-to-roll Production of 30-inch Graphene Films for Transparent Electrodes, *Nat. Nanotech.*, **2010**, 5, 574-578.

3. Tan, W. D. C.; Su,Y.; Knize, R. J.; Xie, G. Q.; Li, L. J.; Tang, D. Y. Mode Locking of

Ceramic Nd:Yttrium Aluminum Garnet with Graphene as a Saturable Absorber, *Appl. Phys. Lett.*, **2010**, 96, 031106.

4. Bao, Q.; Zhang, H.; Wang, B.; Ni, Z.; Xuan Lim, C. H. Y.; Wang, Y.; Tang, D. Y.; Loh, K. P. Broadband Graphene Polarizer, *Nat. Photon.*, **2011**, 5, 411-415.

5. Mueller, T.; Xia, F.; Avouris, P. Graphene Photodetectors for High-Speed Optical Communications, *Nat. Photon.*, **2010**, 4, 297-301.

6. Stauber, T.; Peres, N. M. R.; Geim, A. K. The Optical Conductivity of Graphene in the Visible Region of the Spectrum, *Phys. Rev. B*, **2008**, 78, 085432.

7. Kuzmenko, A. B.; van Heumen, E.; Carbone, F.; van der Marel, D. Universal Optical Conductance of Graphite, *Phys. Rev. Lett.*, **2008**, 100, 117401.

8. Xia, F,; Mueller, T.; Lin, Yu-Ming; Valdes-Garcia, A.; Avouris, P. Ultrafast Graphene Photodetector, *Nat. Nanotech.* **2009**, 4, 839-843.

9. Bonaccorso, F.; Sun, Z.; Hasan, T.; Ferrari, A. C. Graphene Photonics and Optoelectronics, *Nat. Photon.*, **2010**, 4, 611-622.

10. Stuart H. R.; Hall, D. G. Absorption Enhancement in Silicon-on-Insulator Waveguides Using Metal Island Films, *Appl. Phys. Lett.*, **1996**, 69, 2327.

11. Schaadt, D. M.; Feng, B.; Yu, E. T. Enhanced Semiconductor Optical Absorption *via* Surface Plasmon Excitation in Metal Nanoparticles, *Appl. Phys. Lett.*, **2005**, 86, 063106.

12. Cole, A. J. R.; Halas, N. J. Optimized Plasmonic Nanoparticle Distributions for Solar Spectrum Harvesting, *Appl. Phys. Lett.*, **2006**, 89, 153120.

13. Landy, N. I.; Sajuyigbe, S.; Mock, J. J.; Smith, D. R.; Padilla, W. J. Perfect Metamaterial Absorber, *Phys. Rev. Lett.*, **2008**, 100, 207402.

14. Bandiera, Jacob, D.; Muller, T.; Marquier, F.; Laroche, M.; Greffet, J.-J. Enhanced Absorption by Nanostructured Silicon, *Appl. Phys. Lett.*, **2008**, 93, 193103.

15. Teperik, V.; Garcia de Abajo, F. J.; Borisov, A. G.; Abdelsalam, M.; Bartlett, P. N.; Sugawara, Y.; Baumberg, J. J. Omnidirectional Absorption in Nanostructured Metal Surfaces, *Nat. Photon.*, **2008**, 2, 299-301.

16. Driessen, E. F. C.; de Dood, M. J. A. The Perfect Absorber, *Appl. Phys. Lett.*, **2009**, 94, 171109.

17. Kim, K.; Choi, J.; Kim, T.; Cho S.; Chung, H. A Role for Graphene in Silicon-Based Semiconductor Devices, *Nature*, **2011**, 479, 338-344.

18. Liu, M.; Yin, X.; Ulin-Avila, E.; Geng, B.; Zentgraf, T.; Ju, L.; Wang F.; Zhang, X. A Graphene-Based Broadband Optical Modulator, *Nature*, **2011**, 474, 64-67.

19. Li, H.; Anugrah, Y.; Koester S. J.; Li, M. Optical Absorption in Graphene Integrated on Silicon Waveguides, *Appl. Phys. Lett*, **2012**, 101, 111110.

20. Furchi, M.; Urich, A.; Pospischil, A.; Lilley, G.; Unterrainer, K.; Detz, H.; Klang, P.; Andrews, A. M.; Schrenk, W.; Strasser G.; *et al.* Microcavity-Integrated Graphene Photodetector, *Nano Lett.*, **2012**, 12, 2773-2777.

21. Engel, M.; Steiner, M.; Lombardo, A.; Ferrari, A. C.; Loneysen, H. v.; Avouris P.; Krupke, R. Light-Matter Interaction in a Microcavity-Controlled Graphene Transistor, *Nat. Commun.*, **2012**, 3, 906.

22. Ferreira, A.; Peres, N. M. R.; Ribeiro, R. M.; Stauber, T. Graphene-Based Photodetector with Two Cavities *Phys. Rev. B*, **2012**, 85, 115438.

23. Echtermeyer, T. J.; Britnell, L.; Lombardo, A.; Gorbachev, R. V.; Grigorenko, A. N.; Geim, A. K.; Ferrari, A. C.; Novoselov, K. S. Strong Plasmonic Enhancement of Photovoltage in Graphene, *Nat. Commun.*, **2001**, 2, 458.

24. Thongrattanasiri, S.; Koppens, F. H. L.; García de Abajo, F. J. Complete Optical Absorption in Periodically Patterned Graphene, *Phys. Rev. Lett.*, **2012**, 108, 047401.

25. Kravets, V. G.; Grigorenko, A. N.; Nair, R. R.; Blake, P.; Anissimova, S.; Novoselov K.S.; Geim, A. H. Spectroscopic Ellipsometry of Graphene and an Exciton-Shifted van Hove Peak in Absorption, *Phys. Rev. B*, **2010**, 81, 155413.

26. Ferrari, A. C.; Meyer, J. C.; Scardaci, V.; Casiraghi, C.; Lazzeri, M.; Mauri, F.; Piscanec, S.; Jiang, D.; Novoselov, K. S.; *et al.* Raman Spectrum of Graphene and Graphene Layers, *Phys. Rev. Lett.*, **2006**, 97, 187401.

27. Reich, S.; Thomsen, C. Raman Spectroscopy of Graphite, *Phil. Trans. R. Soc. Lond. A*, **2004**, 362, 2271-2288.

28. Gupta, A.; Chen, G.; Joshi, P.; Tadigadapa S.; Eklund, P. C. Raman Scattering from High-Frequency Phonons in Supported n-Graphene Layer Films, *Nano Lett.*, **2006**, 6, 2667-2673.

29. Ni, Z.; Wang, Y.; Yu T.; Shen, Z. Raman Spectroscopy and Imaging of Graphene, *Nano Res.*, **2008**, 1, 273-291.

30. Bludov, Yu. V.; Vasilevskiy, M. I.; Peres, N. M. R. Mechanism for Graphene-Based Optoelectronic Switches by Tuning Surface Plasmon-Polaritons in Monolayer Graphene , *Europhys. Lett.*, **2010**, 92, 68001.

31. Bludov, Yu. V.; Vasilevskiy, M. I.; Peres, N. M. R. Tunable Graphene-Based Polarizer, *J. Appl. Phys.*, **2012**, 112, 084320.

32. Klopfleisch, M.; Golz M.; Trutschel, U. Experimental Verification of a Virtual-Mode Treatment for the Excitation of Surface Plasmon Polaritons by Attenuated Total Reflection, *Appl. Opt.*, **1992**, 31, 5017-5021.

33. Blake, P.; Hill, E. W.; Castro Neto, A. H.; Novoselov, K. S.; Jiang, D.; Yang, R.; Booth, T. J.; Geim, A. K. Making Graphene Visible, *Appl. Phys. Lett.*, **2007**, 91, 063124.

34. Wan, W.; Chong, Y.; Ge, L.; Noh, H.; Stone, A. D.; Cao, H. Time Reversed Lasing and Interferometric Control of Absorption, *Science*, **2011**, 331, 889-892.

35. Chong, Y. D.; Ge, L.; Cao, H.; Stone, A. D. Coherent Perfect Absorbers: Time-Reversed Lasers, *Phys. Rev. Lett.*, **2010**, 105, 053901.

36. Noh, H.; Chong, Y.; Stone, A. D.; Cao, H. Perfect Coupling of Light to Surface Plasmons by Coherent Absorption, *Phys., Rev., Lett.*, **2012**, 108, 186805.

37. Pirruccio, G., Lozano, G.; Zhang, Y.; Rodriguez, S. R. K.; Gomes, R.; Hens Z.; Gomez Rivas, J. *Phys. Rev. B*, Coherent Absortpion and Enhanced Photoluminescence in Thin Layers of Nanorods, **2012**, 85, 165455.

38. Mikhailov S. A.; Ziegler, K. New Electromagnetic Mode in Graphene, *Phys. Rev. Lett.*, **2007**, 99, 016803.

39. Nikitin, Yu. A.; Guinea, F; Garcia-Vidal, F. J.; Martin-Moreno, L. Edge and Waveguide Terahertz Surface Plasmon Modes in Graphene Microribbons, *Phys. Rev., B*, **2011**, 84, 195446.

40. Graphene Supermarket, https://www.graphene-supermarket.com.

41. Li, X.; Zhu, Y.; Cai, W.; Borysiak, M.; Han, B.; Chen, D.; Piner, R. D.; Colombo, L.; Ruoff, R. S. Transfer of Large-Area Graphene Films for High-Performance Transparent Conductive Electrodes, *Nano Lett.*, **2009**, 9, 4359-4363.
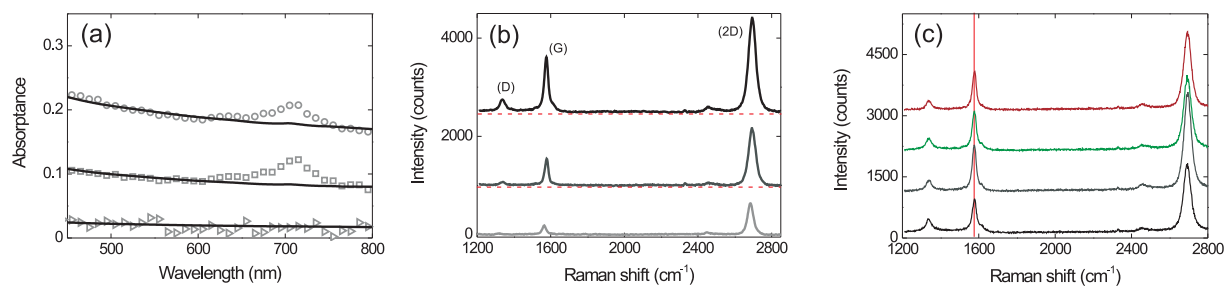
Figure 1: (a) Measured and calculated absorptance of graphene mono- and multi-layers. The measured absorptance is displayed with open circles, squares and triangles for 10 layers, 5 layers and a monolayer of graphene, respectively. The curves correspond to the calculations of the absorptance using the transfer matrix method. (b) Raman spectra of a monolayer (light grey curve), 5 layers (dark grey curve) and 10 layers (black curve) of graphene on a quartz substrate. For clarity, the curves of the 5 and 10 layers have been vertically shifted. Red dashed lines indicate the baseline of the measurements. (c) Raman spectra of the sample with 10 layers of graphene on a quartz substrate taken from 4 different locations in the sample with a large separation (~ 1 nm).
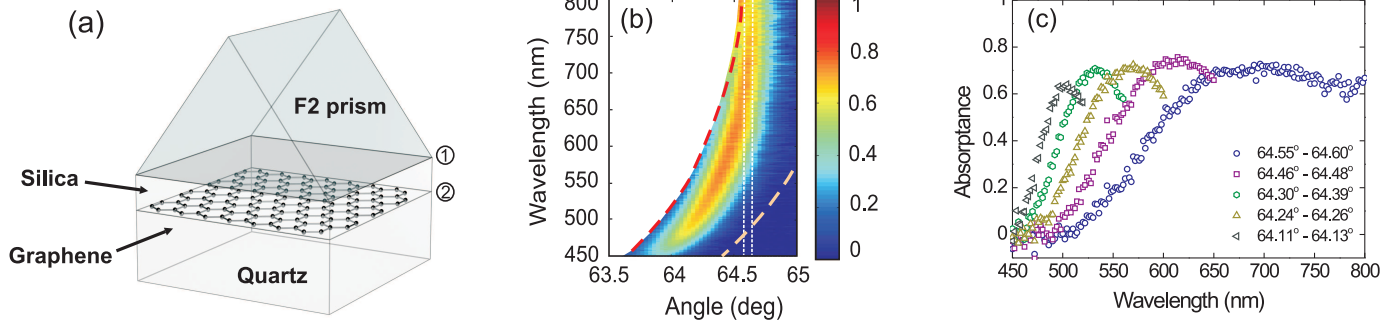
Figure 2: (a) Schematic representation of the multilayer structure formed by a quartz substrate, a graphene layer, a silica layer and a F2 prism. (b) Measured absorptance spectra (color scale) from the structure shown in (a) in which the graphene layer is formed by 5 monolayers randomly stacked. The incident light is p-polarized. The absorptance, evaluated as 1-Reflectance, is displayed as a function of the wavelength and the angle of incidence on the prism-silica interface. (c) Integrated absorptance over the angular ranges $\Delta\theta$ indicated in the legend. The blue dots correspond to the absorptance evaluated in the angular range identified by the dashed white lines in (b).
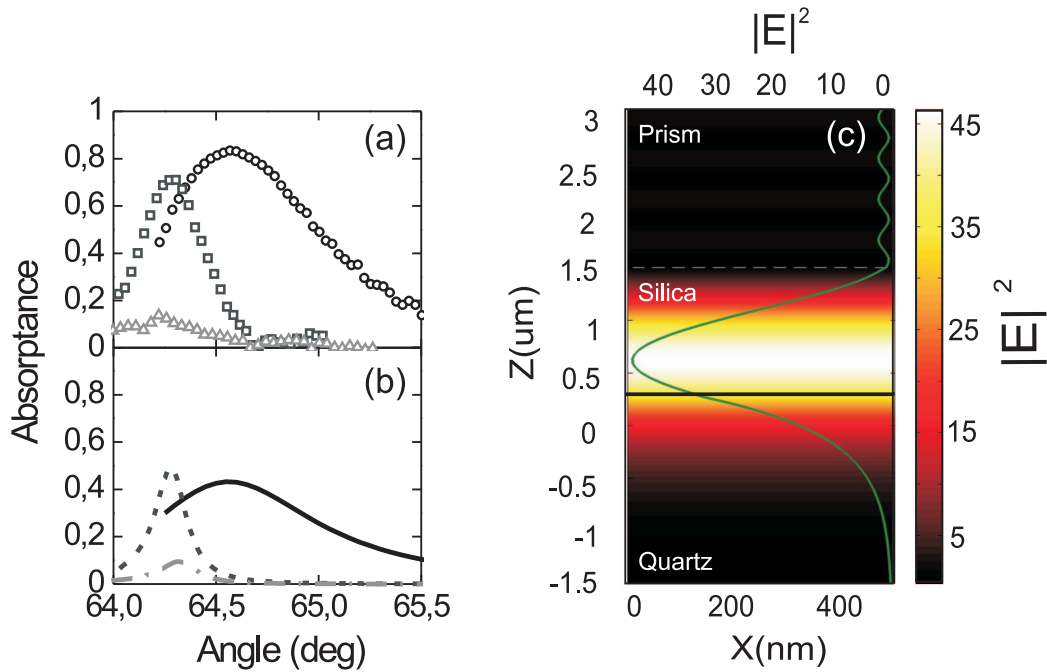
Figure 3: Measured (a) and calculated (b) absorptance spectra as a function of the angle of incidence of a plane wave with a wavelength of 540 nm and for the multilayer system represented in Fig. 2 (a). Open circles and black solid curve correspond to 10 layers of graphene, open squares and dark-grey dotted curve correspond to 5 layers of graphene, and open triangles and grey dash-dotted curve correspond to a monolayer of graphene. (c) Spatial distribution of the total electric field intensity $|E|^2$, normalized by the incident intensity, for the 5-layers graphene sample at $\lambda = 540$ nm and $\theta = 64.3°$. From top to bottom: prism (semiinfinite), silica layer (1200 nm), graphene (solid line) and substrate (semiinfinite). Green curve: $|E|^2$ as a function of z (scale on the upper horizontal axis).
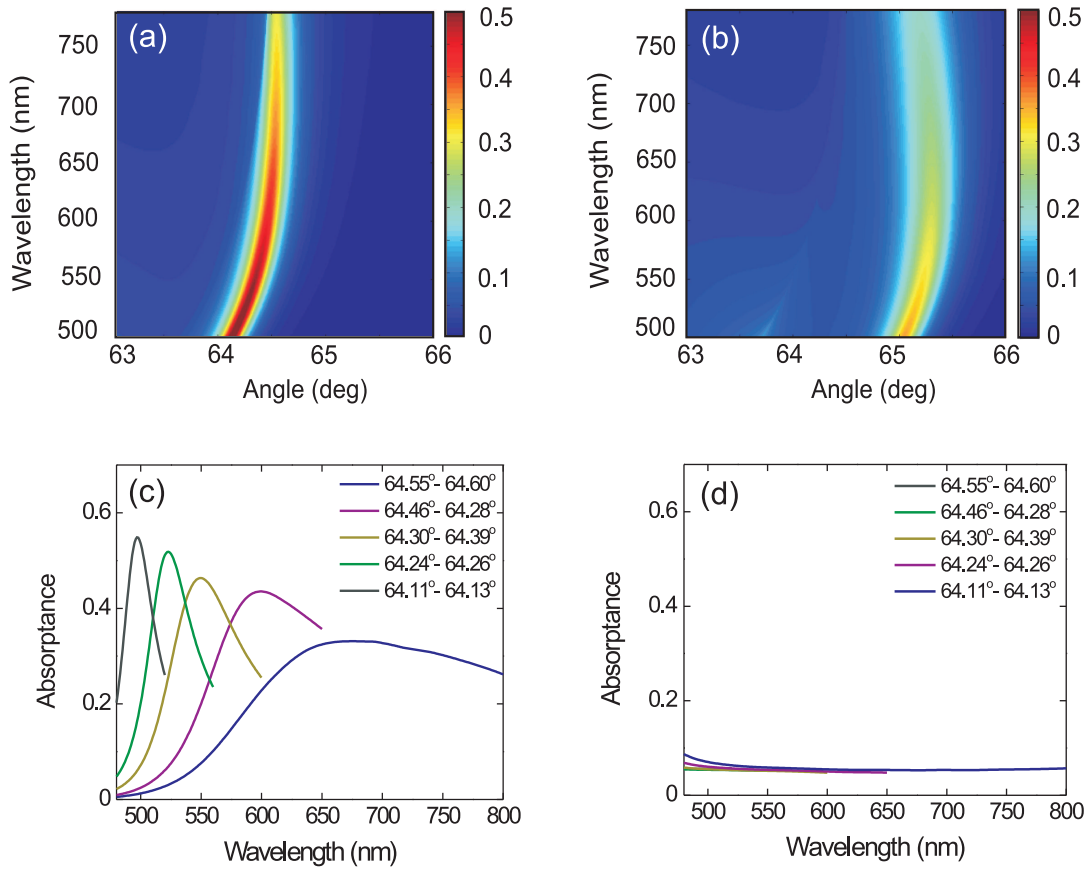
Figure 4: (a) Calculated absorptance as a function of the wavelength and angle of incidence for the 5-layers graphene sample described in Fig 2 (a). (b) Calculated absorptance as a function of wavelength and angle of incidence for the same sample but with $\varepsilon_{silica} = 2.15$ instead of 2.12. (c) and (d) Integrated absorptance calculated from (a) and (b), respectively, over the angular windows indicated in the figure legends.